A Unified Picture of the FIP and Inverse FIP Effects

J. Martin Laming[1]

ABSTRACT

We discuss models for coronal abundance anomalies observed in the coronae of the sun and other late-type stars following a scenario first introduced by Schwadron, Fisk & Zurbuchen of the interaction of waves at loop footpoints with the partially neutral gas. Instead of considering wave heating of ions in this location, we explore the effects on the upper chromospheric plasma of the wave ponderomotive forces. These can arise as upward propagating waves from the chromosphere transmit or reflect upon reaching the chromosphere-corona boundary, and are in large part determined by the properties of the coronal loop above. Our scenario has the advantage that for realistic wave energy densities, both positive and negative changes in the abundance of ionized species compared to neutrals can result, allowing both FIP and Inverse FIP effects to come out of the model. We discuss how variations in model parameters can account for essentially all of the abundance anomalies observed in solar spectra. Expected variations with stellar spectral type are also qualitatively consistent with observations of the FIP effect in stellar coronae.

Subject headings: Sun: corona – stars: coronae

1. Introduction

Element abundance variations observed in the solar corona and wind with respect to those determined for the solar photosphere have proved to be one of the most enduring mysteries of solar physics of the past 15-20 years. The most commonly observed FIP (First

[1]E. O Hulburt Center for Space Research, Naval Research Laboratory, Code 7674L, Washington DC 20375

jlaming@ssd5.nrl.navy.mil

Ionization Potential) Effect refers to the case where elements with first ionization potential below about 10 eV are observed to be enhanced in abundance by a factor of about 3-4 in the solar corona and in the slow speed solar wind. Coronal holes and the fast speed solar wind which emanates from them by contrast show no such fractionation.

Models for such phenomena have come and gone. Early diffusion models based on ion coupling to a background flow of protons (Marsch, von Steiger & Bochsler 1995; Peter 1996; Peter & Marsch 1998; Peter 1998) were shown either to be based on somewhat artificial boundary conditions (McKenzie, Sukhorukova, & Axford 1997; McKenzie 2000), or inherently too slow (Hénoux 1995, 1998). The first FIP effect model to include an external forces acting on the plasma ions that is worked out in some details is that due to Antiochos (1994), based on cross B thermoelectric fields associated with the downward electron flux which gives rise to chromospheric evaporation. The absence of a FIP effect in coronal holes arises naturally, but in coronal regions where FIP fractionation occurs, a mass dependence is predicted which is not observed. More recently two distinct possibilities have been discussed in the literature. Arge & Mullan (1998) proposed that reconnection events in the chromosphere heat ions and not neutrals, the higher ion scale heights then leading to enhanced coronal abundances for those elements which are ionized in the chromosphere, the low FIP elements. A fractionation by a factor of 3-4 arises naturally out of this model; if the reconnection is driven any harder, chromospheric heating ionizes all elements and the distinction between high and low FIP elements is lost. This might be problematic, since higher FIP fractionations are observed in discrete solar features (Feldman & Widing 2003). Less satisfactory is that the difference between corona/slow wind and coronal holes/fast wind is not accounted for. In a qualitatively different approach, Schwadron, Fisk, & Zurbuchen (1999) envisaged a wave heated coronal loop where waves penetrate down to the chromosphere at each footpoint and there selectively heat the ions but not the neutrals, again leading to a positive fractionation of the low FIP species. We remark that the precise nature of the wave heating in their model remains obscure. Ions are heated to a constant velocity, the wave phase speed, by isotropic waves. This would suggest a resonant ion cyclotron heating mechanism. It seems to us that sufficient energy in these waves is unlikely to reach the partially ionized layer of the chromosphere, due to the intrinsically small amount of energy generally believed to reside in high frequency waves, and the damping they would undergo in the partially ionized chromosphere (De Pontieu, Martens, & Hudson 2001). We therefore consider below the effect of nonresonant waves on chromospheric ions, through the action of the ponderomotive force that must exist as Alfvén waves propagate through the chromosphere, either as initially upwards propagating waves impinging on the corona from below, or downward propagating coronal waves impinging of the chromosphere from above. The difference between corona/slow wind and coronal hole/fast wind abundances arises quite naturally in this

model, in that waves on closed loops inevitably return to loop footpoints unless damped or reflected higher up, but waves on open field lines do not. In common with Arge & Mullan (1998), Schwadron, Fisk, & Zurbuchen (1999) only produce a positive FIP fractionation, i.e. only enhancements in abundance of low FIP ions.

This last point has become of great interest with the advent of element abundance measurements in stellar coronae. Feldman & Laming (2000) reviewed the observational situation prior to the launch of Chandra and XMM-Newton. At that time, coronal abundance patterns showed a trend of increasing metal depletion with increasing activity for the most active stars, going from FIP effects in single stars of solar-like activity, through higher activity stars with essentially no coronal abundance anomaly, right up to the most active stars with values of the coronal Fe/H abundance *lower* than solar photospheric values by factors of up to about 3, i.e. a depletion of an order of magnitude compared to low FIP enhanced coronae like that of the Sun. The lowest activity solar-like star, Procyon, also showed no coronal abundance anomaly. With the advent of data from XMM-Newton and Chandra, the elemental abundance anomalies in active stellar coronae were revealed to be more akin to an inverse FIP effect (Brinkman et al. 2001; Drake et al. 2001), in that while high FIP elements are essentially unchanged relative to H, low FIPs are now depleted by typical factors of 1/3. The transition from unfractionated to inverse FIP fractionation with increasing stellar activity is illustrated by Audard et al. (2003). While the ubiquity of the inverse FIP effect remains controversial in many sources due to uncertainties in the underlying photospheric abundances (see discussion in section 4), it appears real enough in at least a few cases to deserve serious consideration. As will be seen in section 5, an inverse FIP effect can also be produced by ponderomotive forces, which is an encouraging sign.

2. The Ponderomotive Force

The ponderomotive force for Alfvén waves has been derived from the term $\vec{j} \times \vec{B}/c = \left(\nabla \times \vec{B}\right) \times \vec{B}/4\pi$ in the MHD momentum equation by Litwin & Rosner (1998). We work from a more general expression for the time-independent ponderomotive force on a particle of species s, f_j^s, given by (Lee & Parks 1983);

$$F_j^s = \frac{1}{16\pi n_s}\left[\left(K^s_{\beta\alpha} - \delta_{\beta\alpha}\right)\frac{\partial E_\alpha E^*_\beta}{\partial x_j} + \frac{\partial}{\partial x_l}\left(\epsilon_{jmp}\epsilon_{klm}\Omega_p \frac{\partial K^s_{\beta\alpha}}{\partial \Omega_k} E_\alpha E^*_\beta\right) - \frac{\partial}{\partial x_l}\left(k_j \frac{\partial K^s_{\beta\alpha}}{\partial k_l}\right) E_\alpha E^*_\beta\right]. \quad (1)$$

Here $K^s_{\beta\alpha}$ are the terms in the dielectric tensor contributed by the species s, $\vec{E}$ and $\vec{E}^*$ are the wave electric field and its complex conjugate, ϵ_{jmp} is the Levi-Cevita symbol, $\vec{\Omega} = q\vec{B}/mc$ where $\vec{B}$ is the magnetic field, q and m are the charge and mass of particles of species s,

c is the speed of light, and $\vec{k}$ is the wavevector. We will consider the simplest possible geometry for a loop footpoint for this initial study, $\vec{B} = (0, 0, B)$ and $\vec{k} = (0, 0, k)$, which means that $\vec{E}$ has only perpendicular (x and y) components for Alfvén or ion cyclotron waves propagating along $\vec{B}$. All plasma quantities are constant in the region of interest, except for $E_\perp$, the particle density, and the ionization fraction of the various elements which may have gradients in the z direction. This means that $l = p = k$ in the second term in equation 1, giving $\epsilon_{klm} = 0$, and hence this term drops out.

We substitute the form of the dielectric tensor derived using the Vlasov approach (Melrose 1986, equation 10.21) to get

$$\begin{aligned} F_j^s &= \frac{1}{16\pi n_s}\frac{4\pi q^2}{m\omega^2}\sum_{p=-\infty}^{\infty}\int \frac{\partial\left|\vec{E}\cdot\vec{V}\right|^2}{\partial z}\frac{1}{\omega - p\Omega - kv_\parallel}\left(\frac{\omega - kv_\parallel}{v_\perp}\frac{\partial f}{\partial v_\perp} + k\frac{\partial f}{\partial v_\parallel}\right) \\ &\quad + \frac{kv_\parallel}{\left(\omega - p\Omega - kv_\parallel\right)^2}\left(\frac{\omega - p\Omega}{v_{t\parallel}^2} + \frac{p\Omega}{v_{t\perp}^2}\right)\frac{\partial f}{\partial z}d^3\vec{v} \end{aligned} \tag{2}$$

where $f = \left(n/v_{t\parallel}v_\perp^2\left(2\pi\right)^{3/2}\right)\exp\left(-v_\parallel^2/2v_{t\parallel}^2 - v_\perp^2/2v_{t\perp}^2\right)$ is the species distribution function in terms of parallel and perpendicular thermal speeds, $v_{t\parallel} = \sqrt{k_\mathrm{B}T_\parallel/m}$ and $v_{t\perp} = \sqrt{k_\mathrm{B}T_\perp/m}$ respectively, parallel and perpendicular velocities $v_\parallel$, $v_\perp$, and particle density n_a. $\left|\vec{E}\cdot\vec{V}\right|^2$ is evaluated to give $E_x^2v_\perp^2\left(J_{p-1} + J_{p+1}\right)^2/4 + E_y^2v_\perp^2\left(J_{p-1} - J_{p+1}\right)^2/4$, where $J_p = J_p\left(k_\perp r\right)$ is the Bessel function of order p with argument $k_\perp r \to 0$ in the MHD approximation. Evaluating in terms of $\phi\left(z\right) = -\left(z/\sqrt{\pi}\right)\int_{-\infty}^{+\infty}\exp\left(-t^2\right)/\left(t - z\right)dt$, the plasma dispersion function, gives

$$\begin{aligned} F_j^s &= \frac{-q^2}{8m\omega^2}\frac{\partial E_\perp^2}{\partial z}\left[\frac{\omega}{\omega-\Omega}\phi\left(\frac{\omega-\Omega}{\sqrt{2}kv_{t\parallel}}\right) + \frac{\omega}{\omega+\Omega}\phi\left(\frac{\omega+\Omega}{\sqrt{2}kv_{t\parallel}}\right) - \left(1 - \frac{v_{t\perp}^2}{v_{t\parallel}^2}\right)\left\{\phi\left(\frac{\omega-\Omega}{\sqrt{2}kv_{t\parallel}}\right) + \phi\left(\frac{\omega+\Omega}{\sqrt{2}kv_{t\parallel}}\right) - 2\right\}\right] \\ &\quad + \frac{q^2E_\perp^2}{8n_sm\omega^2}\frac{\partial n_s}{\partial z}\left\{\frac{\omega v_{t\perp}^2}{v_{t\parallel}^2} + \Omega\left(1 - \frac{v_{t\perp}^2}{v_{t\parallel}^2}\right)\right\}\left\{\frac{\omega-\Omega}{k^2v_{t\parallel}^2}\phi\left(\frac{\omega-\Omega}{\sqrt{2}kv_{t\parallel}}\right) - \frac{\omega-\Omega}{k^2v_{t\parallel}^2} - \phi\left(\frac{\omega-\Omega}{\sqrt{2}kv_{t\parallel}}\right)\frac{1}{\omega-\Omega}\right\} \\ &\quad + \frac{q^2E_\perp^2}{8n_sm\omega^2}\frac{\partial n_s}{\partial z}\left\{\frac{\omega v_{t\perp}^2}{v_{t\parallel}^2} - \Omega\left(1 - \frac{v_{t\perp}^2}{v_{t\parallel}^2}\right)\right\}\left\{\frac{\omega+\Omega}{k^2v_{t\parallel}^2}\phi\left(\frac{\omega+\Omega}{\sqrt{2}kv_{t\parallel}}\right) - \frac{\omega+\Omega}{k^2v_{t\parallel}^2} - \phi\left(\frac{\omega+\Omega}{\sqrt{2}kv_{t\parallel}}\right)\frac{1}{\omega+\Omega}\right\}. \end{aligned} \tag{3}$$

We always have $\omega + \Omega >> \sqrt{2}kv_{t\parallel}$ so $\phi\left(\frac{\omega+\Omega}{\sqrt{2}kv_{t\parallel}}\right) \simeq 1 + k^2v_{t\parallel}^2/\left(\omega+\Omega\right)^2 + 3k^4v_{t\parallel}^4/\left(\omega+\Omega\right)^4 + ...$ Far from a resonance we also have $\omega - \Omega >> \sqrt{2}kv_{t\parallel}$ and making the same approximation for $\phi\left(\frac{\omega-\Omega}{\sqrt{2}kv_{t\parallel}}\right)$ we get (dropping the subscripts/superscript s)

$$F = -\frac{q^2}{4m\left(\omega^2 - \Omega^2\right)}\frac{\partial\left(E_\perp^2\right)}{\partial z} - \frac{q^2E_\perp^2}{2nm\Omega^2}\frac{\partial n}{\partial z}\left(\frac{k^2}{\omega^2}\left(v_{t\parallel}^2 - v_{t\perp}^2\right) + 3\frac{k^2}{\Omega^2}v_{t\parallel}^2\right). \tag{4}$$

For Alfvén waves, $E_\perp^2/8\pi = U_{waves}V_A^2/c^2$ where V_A is the Alfvén speed. Hence $\partial E_\perp^2/\partial z = 8\pi U_{waves}/c^2\partial V_A^2/\partial z = -E_\perp^2/n\partial n/\partial z$, so the three terms in equation 4 are in the ratio 1 :

$2\left(v_{t\|}^2 - v_{t\perp}^2\right)/V_A^2 : 2v_{t\|}^2\omega^2/V_A^2\Omega^2$. For low frequency nonresonant waves the first term always dominates, and hereafter we neglect the second two. As $\omega \rightarrow 0$, we recover the expression of Litwin & Rosner (1998). For wave intensity increasing upwards in the loop footpoint, the first term gives a force directed *downwards* on the ions if $\omega >> \Omega$, and *upwards* if $\Omega >> \omega$. The upwards force is proportional to mass, so the resulting acceleration is mass independent. The reason for such forces lies in the refraction of waves in a density gradient. All waves are refracted towards plasma regions with higher refractive index, which means regions of high density for low frequency waves and regions of low density for high frequency waves. The increased wave pressure in the region of high refractive index produces a force which pushes ions in the plasma towards regions of lower refractive index. This means that low frequency waves push ions to low density regions, i.e. upwards in a gravitationally stratified medium, and high frequency waves push ions towards high density region, i.e. downwards. Close to a resonance $\phi\left(\frac{\omega-\Omega}{\sqrt{2}kv_{t\|}}\right) \simeq (\omega-\Omega)^2/k^2v_{t\|}^2 - (\omega-\Omega)^4/3k^4v_{t\|}^4 + ...$, using $\omega - \Omega << \sqrt{2}kv_{t\|}$, and so

$$F^s = \frac{q^2}{4m\Omega^2}\left[\frac{\partial E_\perp^2}{\partial z}\left(\frac{3}{4} - \frac{v_{t\perp}^2}{2v_{t\|}^2}\right) - \frac{E_\perp^2}{n}\frac{\partial n}{\partial z}\frac{v_{t\perp}^2}{v_{t\|}^2}\right]. \quad (5)$$

Both terms in general give an upwards force on the ions, unless $T_\| >> T_\perp$. Both positive and negative changes in the abundances of ions compared to those of neutrals in the partially ionized region of the chromosphere are possible in the scenario we discuss, but are generally negligible compared to the ponderomotive force due to nonresonant waves. In chromospheric plasma, waves of sufficiently high frequency to produce a downwards ponderomotive force or to resonate with ion gyrofrquencies are rapidly damped by charge exchange collisions (De Pontieu, Martens, & Hudson 2001), and so their effect on abundance fractionation is negligible.

3. The FIP Effect

3.1. Formalism

We follow in part the approach and notation of Schwadron, Fisk, & Zurbuchen (1999). Consider first the motion of ions and neutrals of element s in a background flow of protons and hydrogen with speed u. We neglect the ambipolar force which is generally much less than gravity, and assume a flux tube of constant cross sectional area and magnetic field with height (see e.g. Klimchuk 2000; Watko & Klimchuk 2000) to write the momentum equations for ions and neutrals as

$$\frac{\partial P_{si}}{\partial z} = -\rho_{si}g - \rho_{si}\nu_{si}\left(u_{si} - u\right) \quad (6)$$

$$\frac{\partial P_{sn}}{\partial z} = -\rho_{sn} g - \rho_{sn}\nu_{sn}\left(u_{sn} - u\right), \tag{7}$$

where P_{si} and P_{sn} are the partial pressures of ions and neutrals of element s, ρ_{si} and ρ_{sn} are the corresponding densities, ν_{si} and ν_{sn} the collision rates with ambient gas (assumed hydrogen and protons), u_{si} and u_{sn} the flow speeds, and u the hydrogen flow speed imposed on the loop. We also neglect an inertial term $\partial/\partial z\left(\rho_s u_s^2/2\right)$ since the flow speed is much lower than particle thermal speeds. The momentum equations can be combined to give

$$\frac{\partial P_s}{\partial z} = -\rho_s g - \nu_{eff}\rho_s\left(u_s - u\right) + \frac{\partial \xi_s}{\partial z}\frac{\rho_s v_s^2}{2}\frac{\nu_{si} - \nu_{sn}}{\left(1-\xi_s\right)\nu_{si} + \xi_s\nu_{sn}}, \tag{8}$$

with $\nu_{eff} = \nu_{si}\nu_{sn}/\left(\xi_s\nu_{sn} + \left(1-\xi_s\right)\nu_{si}\right)$ and ξ_s the ionization fraction of element s. For

$$u_s = u - g/\nu_{eff}\left(1 - \mu/m_s\right) + \partial\xi_s/\partial z\left(\rho_s v_s^2/2\right)\left(\nu_{si} - \nu_{sn}\right)/\left\{\left(1-\xi_s\right)\nu_{si} + \xi_s\nu_{sn}\right\} \tag{9}$$

where μ is the mean molecular weight, all elements are lifted by the background flow to the same scale height given by $k_{\rm B}T/\mu g$. This obviously requires $u\nu_{eff} > g$ (assuming the term in $\partial\xi_s/\partial z$ negligible). For $u\nu_s << g$, we get gravitationally stratified solutions with $\rho_s \propto \exp\left(-m_s g z/k_{\rm B}T\right)$. With $g = 2.74\times10^4$ cm s^{-2}, and $\nu_s \sim 10^2 - 10^3$ the former case is valid for the Sun for flow speeds in the chromosphere greater than a relatively modest 10 - 100 cm s^{-1}. The solar wind particle flux at $1R_\odot$ is of order 10^{13} cm^{-2}s^{-1}, which probably requires a flow speed well in excess of 10^3 cm s^{-1} at a density of 10^{10} cm^{-3} (accounting for an unknown area filling factor) to supply it, so we do not expect gravitational separation of elements in the chromosphere.

The solar chromosphere is doubtless a more dynamic environment than represented by equations 6-9. For our purposes the net result of this dynamic behavior is merely to completely mix up the plasma to give uniform elemental composition with height, which is obtained in our model with the above choice for u_s. Other choices may be possible which would provide chemical fractionation in the unperturbed chromosphere, and one could choose u_s to provide the required FIP effect. However the physics behind such a specification for u_s in most cases remains obscure, and is probably unrealistic, leading to an unsatisfactory explanation for the FIP effect. Problems of this sort abound in models where no external force provides the FIP fractionation, as in e.g. Marsch, von Steiger & Bochsler (1995). Our model starts with a fully mixed chromosphere, upon which pondermotive forces due to Alfvén wave reflection and transmission act to provide the fractionation. The low solar chromosphere is of much higher density than the upper layers where the FIP fractionation will occur in our models. Consequently the lower boundary condition of completely mixed photospheric composition material gives an essentially infinite particle "reservoir" to supply the extra fractionated elements.

We now include a ponderomotive force, $\rho_{si}a + b\partial\rho_{si}/\partial z$ (see equations 4 and 5), on the ions in the momentum equations;

$$\frac{\partial P_{si}}{\partial z} = -\rho_{si}g - \rho_{si}\nu_{si}\left(u_{si} - u\right) + \rho_{si}a + b\frac{\partial\rho_{si}}{\partial z} \tag{10}$$

$$\frac{\partial P_{sn}}{\partial z} = -\rho_{sn}g - \rho_{sn}\nu_{sn}\left(u_{sn} - u\right). \tag{11}$$

Taking u_s as specified above and assuming $\partial\left(\xi_s b\nu_{eff}/\nu_{si}\right)/\partial z \simeq 0$ we find

$$\frac{\rho_s\left(z_u\right)}{\rho_s\left(z_l\right)} = \frac{v_s^2\left(z_l\right) + 2b\xi_s\nu_{eff}/\nu_{si}}{v_s^2\left(z_u\right) + 2b\xi_s\nu_{eff}/\nu_{si}} \exp\left\{2\int_{z_l}^{z_u} \xi_s a\nu_{eff}/\nu_{si}/\left(v_s^2 + 2b\xi_s\nu_{eff}/\nu_{si}\right)dz\right\}. \tag{12}$$

A quantitative assessment of coronal element abundances anomalies requires an evaluation of equation 12 with a realistic model chromosphere in the region of Alfvén wave reflection. With $b = 0$, the fractionation produced by the ponderomotive force is proportional to $\exp\left\{2\int_{z_l}^{z_u}\xi_s a\nu_{eff}/\nu_{si}/v_s^2 dz\right\}$ and is approximately mass independent if v_s is dominated by the microturbulent velocity, as it must be if the unperturbed chromosphere is completely mixed with gravitational scale height corresponding to the mean molecular mass. Henceforward we take $b = 0$, following the discussion in section 2.

3.2. Alfvén Wave Reflection

The chromospheric reflection and damping of Alfvén waves has recently been studied in some detail (Ofman 2002; De Pontieu, Martens, & Hudson 2001) in connection with observations by TRACE of the damping of loop oscillations (Nakariakov et al. 1999). Waves with frequency below the ion-neutral charge exchange rate propagate essentially undamped through chromospheric plasma, but can be reflected at the chromosphere-corona boundary.

When the Alfvén wavelength is much larger than the characteristic length scale over which the density changes, the amplitude reflection coefficient is given approximately by $B_r/B_i = \left(V_{A1} - V_{A2}\right)/\left(V_{A1} + V_{A2}\right)$, where V_{A1} and V_{A2} are the Alfvén speeds of the incident and transmitted wave respectively. Since B is continuous across the boundary, $B_t = B_r + B_i$ and $B_t/B_i = 2V_{A1}/\left(V_{A1} + V_{A2}\right)$. These simple results are recovered in the long wavelength limit when the chromosphere is treated as an exponential atmosphere (Leroy 1980; Ofman 2002). The wave magnetic field in this case can be expressed in terms of Hankel fuctions (Hollweg 1984; De Pontieu, Martens, & Hudson 2001) with argument $\left(2h\omega/V_{Ac}\right)\exp\left(-z/2h\right)$, where h is the chromosphere scale height, $V_A = V_{Ac}\exp\left(z/2h\right)$ is the chromospheric Alfvén speed, in terms of its (assumed constant) coronal value V_{Ac} and $z\,(<0)$ is the depth below the corona. When $\left(2h\omega/V_A\right)\exp\left(-z/2h\right) << 1$ (the long wavelength limit) the expression

can be simplified by expressing the Hankel functions in terms of Bessel functions and taking the appropriate limits when the arguments are much less than unity. The result is

$$B_\perp = \frac{irB_0}{V_{Ac}} \left[(e+f)\,\frac{\alpha}{2} \exp\left(-z/h\right) - i\,(e-f)\,\frac{2}{\pi\alpha} \right] \exp\left(i\omega t\right), \tag{13}$$

where $\alpha = 2h\omega/V_{Ac}$, B_0 is the longitudinal (static) magnetic field, r is the radius of the assumed torsional oscillation, and e and f are complex constants representing the magnetic field amplitude of the upward and downward propagating chromospheric waves respectively. So long as the Alfvén wave energy flux through the chromosphere is nonzero (i.e. $e \neq f$), with $\alpha \sim 10^{-3} - 10^{-2}$ for solar parameters, $B_\perp$ and the wave energy density $B_\perp^2/8\pi$ are essentially independent of z in all regions except the lowest chromospheric levels. Making the identification $U_{waves} = B_\perp^2/8\pi = c^2 E_\perp^2/8\pi V_A^2$, for the wave energy density we deduce

$$\frac{\partial E_\perp^2}{\partial z} = \frac{V_A}{c^2} 16\pi U_{waves} \frac{\partial V_A}{\partial z} = \frac{V_A^2}{c^2} \frac{8\pi U_{waves}}{h}. \tag{14}$$

The ponderomotive acceleration is then $a = U_{waves}/2h\rho \simeq 2.5 \times 10^4$ cm s^{-2} for $U_{waves} = 0.1$ erg cm^{-3}, $h = 200$ km and $\rho = 10^{-13}$ g cm^{-3}. More realistic chromospheric models employed below (Vernazza, Avrett, & Loeser 1981) have steeper density gradients in certain regions, giving even stronger ponderomotive acceleration. If sufficient cancelation exists between e and f so that the first term in equation 13 dominates, $B_\perp \propto \exp\left(-z/h\right)$ and $E_\perp \propto \exp\left(-z/2h\right)$, giving a ponderomotive force on ions directed downwards. The possibility that solutions of this type might play a role in the inverse FIP effect is discussed in more detail below.

3.3. Simulations

We calculate the wave energy gradient using the results above in the model chromospheres of Vernazza, Avrett, & Loeser (1981). Atomic data for ionization and recombination rates are taken from the compilation of Mazzotta et al. (1998), including rates due to charge transfer recombination and ionization from Kingdon & Ferland (1996). Photoionization rates are evaluated using fits to cross sections in Verner et al. (1996). At each layer of the chromosphere, the average solar spectra of Vernazza & Reeves (1978) and Malinovsky & Heroux (1973) are attenuated by absorption by atomic hydrogen, and then used to compute the photoionization rates for neutral species, which together with collisional ionization and recombination rates are used to calculate the ionization fractions of the various elements. Plots of the ionization fraction of O, Ne, Si, and Ar against height above the photosphere coming from our models are given as solid lines in Figure 1. The long dashed line gives the

H ionization fraction in the VALC model, and the short dashed line gives the temperature in the model. All other low FIP elements are virtually indistinguishable on this plot to Si, i.e. all retain ionized fractions very close to unity for the range of heights shown. The O ionization balance follows that of H very closely because of the fast charge exchange rates between O and H. This is due to the close correspondence between their first ionization potentials.

We evaluate equation 12 integrating the VALC model, corresponding to average quiet sun, through the chromosphere. The ponderomotive acceleration is calculated from the gradient of the Alfvén speed in the VALC chromospheric model and equation 14. This is not completely self-consistent, since equation 14 is derived assumed an exponential atmosphere, not the VALC model, but should be adequate for the purposes of this paper. The ion-proton elastic collision rate is given by the standard Spitzer formula and is numerically:

$$\nu_{\rm ion-p} = \frac{3.1 \times 10^4}{A} \left(\frac{T}{10^4 {\rm K}} \right)^{-3/2} \left(\frac{n_p}{10^{10} {\rm cm}^{-3}} \right) \quad {\rm s}^{-1}. \tag{15}$$

Collision rates where one or both particles are neutral are calculated from the effective cross sections given in Vauclair & Meyer (1985, and tabulated for reference in Table 1), assumed constant with proton or hydrogen velocity. Formally, such behavior arises in the limit that the scattering particle wavefunction is much larger than the range of the scattering potential (see e.g. Landau & Lifshitz 1977). Protons at 10^4 K have de Broglie wavelengths of about 4 Å , to be compared with typical atomic size or potential ranges of about 2 Å . The numerical value is

$$\nu_{\rm ion-H} \simeq \frac{9.1 \sigma_{15}}{A} \left(\frac{T}{10^4 {\rm K}} \right)^{1/2} \left(\frac{n_H}{10^{10} {\rm cm}^{-3}} \right) \quad {\rm s}^{-1}, \tag{16}$$

where $\sigma_{15} \sim 1$ is the scattering cross section in units of 10^{-15} cm^2. Previous authors (von Steiger & Geiss 1989; Marsch, von Steiger & Bochsler 1995; Schwadron, Fisk, & Zurbuchen 1999) have used formulae for ion-hydrogen and proton-neutral collision rates involving the static atomic polarizability which give collision rates larger by a factor typically about 2. In equations 6-11, $\nu_{si} = \nu_{ion-p} + \nu_{ion-H}$ and $\nu_{sn} = \nu_{ion-H} \, (1 + n_p/n_H)$. We estimate ν_{sn} for other elements by scaling from values given in Table 1 using tabulated values of static polarizabilities for neutral atoms of the various elements in Lide (1995).

We give in Table 2 the FIP fractionation for a variety of elements computed for the VALC background model for Alfvén wave energy densities ranging between 0.01 and 0.1 ergs cm^{-3}, corresponding to non-thermal mass motions of up to 10 km s^{-1} at a density of 10^{11} cm^{-3}. At an energy density of 0.04 ergs cm^{-3}, we find a very encouraging correspondence between our model values and observational values taken from the reviews of Feldman & Laming (2000) and Feldman & Widing (2003). In particular an almost mass independent fraction of around

3 occurs for Mg, Si, Fe, and Ni. The very low FIP and extremely reactive elements Na and K show fractionations of 5.42 and 7.22 respectively, also consistent with observations. Of the high FIP elements (excluding S), Ar has the highest abundance enhancement of 1.25. S is something of a special case, being the high FIP element with the lowest FIP of 10.36 eV. Our model gives it an intermediate behavior, with a FIP fractionation of 1.93. Al and Ca are predicted to have similar mass independent fractionation to Mg, Si, and Fe, whereas observations indicate a behavior more like Na and K. This discrepancy would probably be resolved by improved atomic data for neutral-H collisions for these elements. We emphasize that given the background model and the atomic data, there is *only one free parameter* in all these models, namely the Alfvén wave energy density. Insignificant fractionation between H and He occurs in our model. The abundance ratio He/H has recently been measured in regions of quiet solar corona (Laming & Feldman 2003) to be similar to that observed in the slow speed solar wind, i.e. in the range 0.04-0.05 instead of the value inferred for the solar envelope by helioseismology of 0.085 (Basu 1998; Kosovichev 1997). The He/H abundance ratio in the solar wind is observed to be quite variable over the course of the solar cycle (Aellig, Lazarus, & Steinberg 2001a,b), and these variations are not present in the FIP fractionation of other elements. Consequently, one should not expect the physical mechanisms that produce the FIP effect to be responsible for the He fractionation.

Different VAL models produce different FIP fractionations. For 0.04 ergs cm^{-3} wave energy density, runs for the Si FIP fractionation which with VALC is given in Table 2 as 3.42, VALA gives 30.2, VALB 6.59, VALD 2.56, VALE 2.02 and VALF give 1.69. These models range from a dark point within a cell (VALA), an average cell center (VALB), average quiet sun (VALC),average network (VALD), a bright network element (VALE) and a very bright network element (VALF).

We have extended the elements we consider beyond the list of those usually of interest to spectroscopists to include Kr, Rb and W. Modest increases in the wave energy density from that which gives the observed quiet sun FIP fractionation produce enormous increases in the abundances of Rb and W, which may be of relevance to element abundances in some impulsive solar energetic particle events. Kr on the other hand, behaves like the other high FIP elements. The ^{3}He abundance enhancements of factors $10^3 - 10^4$ in such events are relatively well known. More modest abundance enhancements of heavy elements are also seen, e.g. Fe is observed enhanced relative to O by a factor ~ 10 over usual coronal abundances. This is usually interpreted as being due to more efficient stochastic acceleration of ions with lower charge to mass ratios, i.e. those ions with longer gyroradii. Such acceleration occurs in the flare loop rather than in the chromosphere. Going to elements heavier than Fe, even stronger anomalies have recently been found (Reames 2000). Measurements with the Wind/EPACT/LEMT (Energetic Particle Acceleration, Composition and Transport/Low

Energy Matrix Telescope) instrument reveal elements with $34 \leq Z \leq 40$ overabundant by a factor ~ 100 and those with $50 \leq Z \leq 56$ overabundant by ~ 1000, relative to coronal values. These anomalies are similar in magnitude to those for ^{3}He. The ACE/ULEIS (Advanced Composition Explorer/Ultra Low Energy Isotope Spectrometer) instrument reveals similar anomalies going out as far as Bismuth ($Z = 83$). If these abundance anomalies were related to the FIP effect under discussion here, we would expect $34 \leq Z \leq 40$ bin to be dominated by the very low FIP elements Rb, Sr, Y, etc, with Kr remaining essentially unchanged and the bin at $50 \leq Z \leq 56$ to be dominated by Cs and Ba. Some FIP selectivity is evident around atomic masses corresponding to Kr, Rb, Sr, etc in recent observations of SEP ultra-heavy ions in impulsive solar flares (Mason et al. 2004, their figure 6), but the data appear to be in better agreement with our computed values for wave energy densities around 0.04 ergs cm^{-3}, rather than the higher values. Data around Xe, Cs, and Ba are noisier, but show essentially no FIP selectivity. We emphasize that the degree of fractionation depends on the assumption that in the chromosphere unperturbed by Alfvén wave reflection, these elements are sufficiently coupled to the background flow to rise up to the same gravitational scale height as H and the other elements, and that this might be questionable for these, the heaviest of the elements in our sample. Some gravitational settling of heavy elements does appear to be in evidence in the solar photosphere and convection zone, as indicated by the disagreement between recent spectroscopic photospheric abundance measurements and determinations from helioseismology (Bahcall & Pinsonneault 2004; Asplund et al. 2004).

4. Alfvén Wave Reflection Revisited and Variation in the FIP Effect

Before proceeding to discuss how variations of the FIP fractionation, including the possibility of an inverse FIP effect, might arise, we consider in more detail the properties of Alfvén waves in the chromosphere. Hollweg (1984) modeled the transmission of Alfvén waves from the chromosphere into the corona using a three layer loop model; a coronal midsection anchored in the chromosphere at each end. Waves are fed in at one end, may undergo reflection or transmission each time they encounter a chromosphere-corona boundary, and can leak out of the other footpoint. In Figure 3 we show the transmission coefficient into the corona for upward propagating waves in the chromosphere (lower panel). The results are calculated for a model with chromospheric scale height $h = 2 \times 10^7$ cm, coronal Alfvén speed $V_{Ac} = 10^8$ cm s^{-1}, and loop length $d = 10^{10}$ cm (solid curves), and for a coronal hole where the limit $d \rightarrow \infty$ is taken (dashed curves; Hollweg's two-layer model). The upper panel shows the associated wave magnetic field at the corona-chromosphere boundary, in units of the initial upward wave amplitude e expressed as a fraction of the unperturbed magnetic field strength B and the radius of the torsional oscillation r. The strongest wave magnetic field,

and hence energy density and ponderomotive force, are clearly associated with the maxima in the Alfvén wave transmission. From the difference in the plots for a closed loop and the coronal hole, we see that most of the waves responsible for the FIP fractionation must be of relatively low frequency close to the loop fundamental near a period of 200 s, in order for different fractionations to appear in each case. At higher frequencies corresponding higher order harmonics of the loop, the difference in wave magnetic field between the closed loop and coronal hole is rather small, and less obviously capable of producing different fractionations. The Alfvén wave energy density represented by the plots in Figure 3 is nearly 6 times higher in the closed loop than in the coronal hole assuming a flat wave spectrum between 10 and 1000 s periods. In the range between 100 and 1000 s period, the closed loop has a factor 20 more wave energy density. With reference to Table 2, these differences are more than sufficient to produce the observed abundance differences. Note that in each case we have assumed the same wave amplitude incident from below.

If it is the case that the solar FIP effect in coronal loops is due to the approximate equality of wave frequencies generated within the convection zone and hence the chromospheric Alfvén wave spectrum (see e.g. Hathaway et al. 2000; McAteer et al. 2004), and the resonant frequencies of coronal loops, then a number of other predictions should follow. First, the FIP enhancement in any particular solar loop should depend on its size. This does indeed appear to be the case, in that the small loops reaching maximum temperatures below 10^6 K (the unresolved fine structures Feldman 1983, 1987) do have element compositions resembling the solar photosphere (Laming, Drake & Widing 1995), whereas larger higher temperature loops show the usual FIP effect. This is presumably because these smaller loops have resonant frequencies too high for efficient Alfvén wave transmission to their higher temperature regions. Further, the FIP effect in stars of different spectral type might also show interesting variations from the solar case. Stars of earlier type than the Sun (G2V) will have shallower convection zones, and are generally thought to have lower coronal magnetic fields. Consequently the chromospheric Alfvén wave spectrum might be expected to be of higher frequency than that in the Sun, while the resonant frequencies of coronal loops are lower, more similar to solar coronal holes. The observed absence of the FIP effect in the corona of Procyon (F4IV; Drake et al. 1995; Drake, Laming & Widing 1995; Raassen et al. 2002; Sanz-Forcada, Favata, & Micela 2004) is indicative of such an example. Going to later spectral type than the Sun, the deeper convection zones generate lower frequency chromospheric waves, but also higher coronal magnetic fields leading to a mismatch in the opposite sense, i.e. the coronal loop resonant frequency is higher than the chromospheric wave spectrum leading again to inefficient wave transmission and reduced abundance enhancements. FIP effects reduced in magnitude compared to that in the Sun, but not absent, are seen in ϵ Eridani (K2V; Laming, Drake & Widing 1996; Sanz-Forcada, Favata, & Micela 2004), and α

Cen AB (G2V and K1V; Drake, Laming & Widing 1997; Raassen et al. 2003a), while ξ Boo A (G8; Laming & Drake 1999; Drake & Kashyap 2001), π^1UMa (G1V) and χ^1Ori (G0V; Güdel et al. 2002) show similar FIP fractionation to the solar corona.

It is less clear what the correspondence between upward propagating chromospheric wave frequencies and resonant frequencies of coronal loops should be in interacting binary stars such as RSCVn and Algol-type binaries. Observationally, the pre-Chandra/XMM-Newton view of essentially zero coronal abundance fractionation at the low end of the activity scale for these objects going over to inverse FIP effect or metal depletion at the high reviewed by Feldman & Laming (2000) still holds true, with the caveat raised recently by Sanz-Forcada, Favata, & Micela (2004), that fewer and fewer of these stars seems to exhibit true metal depletion in their coronae, the coronal abundance merely reflecting metal poor photospheres. However metal depleted coronae, or inverse FIP effect, does appear to exist in some cases, e.g. II Peg (K2IV plus an unseen companion; Huenemoerder, Canizares & Schultz 2001), AR Lac (G and K subgiants in a 1.98 day orbit; Huenemoerder et al. 2003) and AB Dor (K2 IV-V with a 0.515 day spin period; Sanz-Forcada, Maggio & Micela 2003). Further, the variation of element abundance during stellar flares, in which initially metal depleted plasma evolves towards the standard composition, interpreted in terms of the chromospheric evaporation of unfractionated plasma to the coronal flare site, seems to require the existence of such abundance anomalies. Such phenomena are observed in HR 1099 (K1 IV and G5 IV; Audard, Güdel, & Mewe 2001), Algol (B8 V and K2 IV; Favata & Schmitt 1999), and UX Ari (G5 V and K0 IV; Güdel et al. 1999) where the later type subgiant is taken to be the main source of coronal emission, as well as AB Dor (Güdel et al. 2001a), YY Gem (dMe and dMe with 0.814 day orbit; Güdel et al. 2001b), II Peg(Mewe et al. 1997), and AT Mic (dM4.5 and dM4.5; Raassen et al. 2003b).

Hollweg (1984) argues further that some coronal dissipation of the Alfvén waves must exist, in order to overestimating the nonthermal line broadening. The inclusion of wave damping does not qualitatively change our considerations, except that for increased damping the difference in wave properties between coronal holes and closed loops becomes smaller. Only at wave damping rates beyond the validity of Hollweg's analytic treatment does this difference actually disappear.

In Figure 4 we plot the variation of the wave electric field (upper panel) and magnetic field (lower panel) with distance through the chromosphere below the corona. A positive gradient of wave electric field gives an upwards ponderomotive force, and is realized in all cases close to the coronal boundary. At a wave period of 207 s, corresponding to the loop fundamental frequency, the upwards force is strongest and is present at all heights. For most chromospheric heights the off resonant waves, corresponding to the magnetic field minimum

at wave period 408 s gives decreasing wave electric field with increasing height, which would lead to a downwards ponderomotive force on the ions. This is discussed further below in the subsection on the inverse FIP effect. Away from these two limiting cases, the chromospheric wave fields generally show negative gradient of electric field at low heights and a positive gradient higher up. In our simulations above with hopefully more realistic chromospheric density profiles coming from VAL models, most FIP fractionation occurred within 200 km of the chromosphere-corona boundary, and so we should expect a closed loop excited by a broad spectrum of Alfvén waves below to generally show a positive FIP enhancement. However it is not absolutely clear that the top of the chromosphere in VAL models can be identified with the chromosphere-corona boundary in Hollweg's model, which really marks a transition from an exponentially stratified atmosphere to a uniform density corona, and might reasonably be taken to indicate the top of the transition region instead.

5. The Inverse FIP Effect?

We now consider possibilities arising with wave reflection in the chromosphere to produce a so-called Inverse FIP effect. We mentioned above that high frequency waves from the corona capable of producing a downwards ponderomotive force on ions are likely to be heavily damped by charge exchange in the partially neutral chromosphere. Even the lower charge exchange rates in molecular as opposed to atomic gas do not allow sufficient ponderomotive forces, even for wave energy densities in the range up to 1 erg cm^{-3}. Further, a ponderomotive acceleration produced by such waves would not in general be mass independent, in conflict with observations (see e.g. Audard et al. 2003; Sanz-Forcada, Favata, & Micela 2004).

We instead turn our attention to the most direct "inverse" of the model outlined above. Alfvén waves coming up from the stellar convection zone can be reflected back down again unless they are of the precise frequency to be transmitted all the way into the corona (Hollweg 1984; De Pontieu, Martens, & Hudson 2001). Taking the corona-chromosphere boundary in Hollweg's model to represent the true top of the chromosphere, then to have a downwards ponderomotive force just below this region, we require from equation 13 an almost zero net Alfvén wave energy flux through the chromosphere, i.e. complete reflection at the chromosphere-corona boundary to give $e = f$. In this case the wave energy density $B_\perp^2/8\pi \propto \exp(-2z/h)$ and $E_\perp^2 = V_A^2 B_\perp^2/c^2 \propto \exp(-z/h)$. The gradient of $E_\perp^2$ is now directed downwards,

$$\frac{\partial E_\perp^2}{\partial z} = -\frac{V_A^2}{c^2}\frac{8\pi U_{waves}}{h} \tag{17}$$

giving the ponderomotive force necessary for an inverse FIP effect. This cancellation between these two terms is the origin of the inverse FIP effect found above at the wave period of

408 s corresponding to the minimum wave magnetic field. From equation 13, we see that we require $e - f << (e + f)\,\alpha^2 \exp(-z/h)$ which for a chromosphere similar to that of the sun ($\alpha \sim 0.01$) requires cancelation between c and d to an accuracy of 10^{-4} close to $z = 0$, where most fractionation occurs in our models.

This cancelation condition requires an almost complete reflection of waves upon first encountering the corona from below, which can be shown analytically and numerically to practically never occur within Hollweg's model. The cancelation condition may only be achieved if waves are fed in from each chromospheric footpoint with the same amplitude and phase. This is probably more likely in stars with lower gravity, and hence larger chromospheric scale heights, where the degree of cancelation required is significantly lower.

A further condition required to achieve wave cancellation in the chromosphere with waves fed in from both footpoints is that there should be negligible wave dissipation in the corona. Hollweg (1984) shows that in the solar case some coronal wave dissipation is necessary to avoid predicting unrealistically high non thermal line broadening. We speculate that chromospheric incident waves with lower frequencies relative to those in the sun will need to turbulently cascade to higher relative frequencies to dissipate if the coronal magnetic field is higher, and that this extra decade or two in frequency reduces the dissipation to sufficiently low levels. Constraints on non thermal line broadening are much less stringent in stars exhibiting the inverse FIP effect, due to their rapid rotation.

We speculate that a more realistic chromospheric density and Alfvén wave profile would yield a more robust inverse FIP effect. In particular, if the region of FIP or inverse FIP fractionation could be identified not with the region just below the chromosphere-corona boundary in Hollweg's model, but lower down (i.e. $z \sim -\text{few} \times h$ instead of $z \sim 0$) then downwards ponderomotive forces could be more prevalent. Stars with copious low frequency Alfvénic turbulence could then routinely show inverse FIP effects. This would obviate the need for waves being fed into both loop footpoints, and reduce the degree of cancellation required between upward and downward propagating waves. Such turbulence is likely to derive from differential rotation of the envelope rather than from convection, in order to provide the necessary low frequency waves, and to match the observational constraint that inverse FIP effects generally appear only in rapidly rotating stars.

We close this section by commenting that Schwadron, Fisk, & Zurbuchen (1999) also give a mechanism for inverse FIP effects. The combination of upwards force due to the partial pressure of neutrals and downwards force due to the partial pressure of ion has the effect of enhancing the coronal abundance of high FIP ions since they ionize higher up than the low FIP elements. However quantitative considerations indicate that such fractionation only occurs for flow speeds in the coronal section of the loop much less than 1 km s^{-1} (in

section 3.1 above we discussed flow speeds through the chromosphere). At a more realistic flow speed of 1-10 km s^{-1}, all fractionation disappears.

6. Conclusions

In this paper we have attempted to demonstrate that the ponderomotive force arising as Alfvén waves propagate through the chromosphere of the Sun or stars can give rise to the by now well documented coronal element abundance anomalies. The upward ponderomotive force on ions that produces the FIP effect turns out to be relatively robust for solar parameters, and most likely diminishes as one moves either up or down in stellar activity from the Sun. The absolute magnitude of the fractionation produced depends sensitively on the chromospheric wave energy density. There is nothing "magic" about the solar FIP fractionation of a factor of 3-4; in the presence of higher or lower wave energy densities higher or lower FIP fractionations will be seen. As well as providing a successful quantitative account of the solar FIP effect and its variations, an inverse FIP effect may also come out of the same model. The main simplifying assumptions we have employed in this work are that the magnetic field is constant with height in the chromospheric loop footpoints, the Alfvén waves propagate only along the magnetic field (but in both directions), and that the vertical structure of the chromosphere can be described by the models of Vernazza, Avrett, & Loeser (1981) with no fractionation in the absence of ponderomotive forces. Using observed coronal spectra we have calculated the various element ionization fractions in the chromosphere, and using equation 14 we have evaluated the ponderomotive acceleration and resulting FIP fractionation. Once fully understood, coronal abundance anomalies may offer a unique diagnostic of Alfvén wave propagation between the solar/stellar chromosphere and corona.

This work has been supported by NASA Grant NAG5-9105, by NASA Contract S13783G, and by the NRL/ONR Solar Magnetism and the Earth's Environment 6.1 Research Option. I am indebted as ever to my colleagues Jeremy Drake and Jim Klimchuk for encouragement, advice and useful references.

REFERENCES

Aellig, M. R., Lazarus, A. J., & Steinberg, J. T. 2001, Geophys. Res. Lett., 28, 2767

Aellig, M. R., Lazarus, A. J., & Steinberg, J. T. 2001 in AIP Conference Proceedings 598, Solar and Galactic Composition, ed. R. F. Wimmer-Schweingruber, p89

Antiochos, S. K. 1994, Adv. Space Res., 14, 139

Arge, C. N., & Mullan, D. J. 1998, Solar Physics, 182, 293

Asplund, M., Grevesse, N., Sauval, A. J., Allende Prieto, C., & Kiselman, D. 2004, A&A, in press, astro-ph/031229

Audard, M., Güdel, M., & Mewe, R. 2001, A&A, 365, L318

Audard, M., Güdel, M., Sres, A., Raassen, A. J. J., & Mewe, R. 2003, A&A, 398, 1137

Bahcall, J. N., & Pinsonneault, M. H. 2004, Phys. Rev. Lett., submitted, astro-ph/0402114

Basu, S, 1998, MNRAS, 298, 719

Brinkman, A. C., et al. 2001, A&A, 365, L324

De Pontieu, B., Martens, P. C. H., & Hudson, H. S. 2001, ApJ, 558, 859

Drake, J. J., Brickhouse, N. S., Kashyap, V., Laming, J. M., Huenemoerder, D. P., Smith, R., & Wargelin, B. 2001, ApJ, 548, L81

Drake, J. J., & Kashyap, V. 2001, ApJ, 547, 428

Drake, J. J., Laming, J. M., Widing, K. G., Schmitt, J. H. M. M., Haisch, B., & Bowyer. S. 1995, Science, 267, 1470

Drake, J. J., Laming, J. M., & Widing, K. G. 1995, ApJ, 443, 393

Drake, J. J., Laming, J. M., & Widing, K. G. 1997 ApJ478, 403

Favata, F., & Schmitt, J. H. M. M. 1999, A&A, 350, 900

Feldman, U. 1983, ApJ, 275, 367

Feldman, U. 1987, ApJ, 320, 426

Feldman, U., & Laming, J. M. 2000, Physica Scripta, 61, 222

Feldman, U., & Widing, K. G. 2003, Space Science Reviews, 107, 665

Güdel, M., Audard, M., Sres, A., Wehrli, R., Behar, E., Mewe, R., Raassen, A. J. J., & Magee, H. R. M. 2002, in Stellar Coronae in the Chandra and XMM-Newton Era, eds F. Favata & J. J. Drake, ASP Conf. Ser. 277, 497

Güdel, M., Audard, M., Briggs, K., Haberl, F., Magee, H., Maggio, A., Mewe, R., Pallavicini, R. & Pye, J. 2001a, A&A, 365, L336

Güdel, M., Audard, M., Magee, H., Franciosini, E., Grosso, N., Cordova, F. A., Pallavicini, R., & Mewe, R. 2001b, A&A, 365, L344

Güdel, M., Linsky, J. L., Brown, A., & Nagase, F. 1999, ApJ, 511, 405

Hathaway, D. H., Beck, J. G., Bogart, R. S., Bachmann, K. T., Khatri, G., Petitto, J. M., Han, S., & Raymond, J. 2000, Solar Physics, 193, 299

Hénoux, J.-C. 1995, Adv, Space Res., 15, 23

Hénoux, J.-C. 1998, Space Science Rev., 85, 215

Hollweg, J. V. 1984, ApJ, 277, 392

Huenemoerder, D. P., Canizares, C. R., Drake, J. J., & Sanz-Forcada, J. 2003, ApJ, 595, 1131

Huenemoerder, D. P., Canizares, C. R., & Schultz, N. S. 2001, ApJ, 559, 1135

Kingdon, J. B., & Ferland, G. J. 1996, ApJS, 106, 205

Klimchuk, J. A. 2000, Sol. Phys. 193, 53

Kosovichev, A. 1997, in AIP Conf. Proc. 385, Robotic Exploration Close to the Sun: Scientific Basis, ed. S. R. Habbal (Woodbury: AIP), 159

Laming, J. M., Drake, J. J., & Widing, K. G. 1995, ApJ443, 416

Laming, J. M., Drake, J. J., & Widing, K. G. 1996, ApJ, 462, 948

Laming, J. M. & Drake, J. J. 1999, ApJ, 516, 324

Laming, J. M., & Feldman, U. 2003, ApJ, 591, 1257

Landau, L. D., & Lifshitz, E. M. 1977, Quantum Mechanics (Non-relativistic Theory), (Oxford: Pergamon Press), pp542

Lee, N. C., & Parks, G. K. 1983, Phys. Fluids, 26, 724

Leroy, B. 1980, A&A, 91, 136

Lide, D. R. (ed) 1995, CRC Handbook of Chemistry and Physics, 76th Edition (Boca Raton, Fl: CRC Press Inc.)

Litwin, C., & Rosner, R. 1998, ApJ, 506, L143

Malinovsky, M., & Heroux, L. 1973,ApJ, 181, 1009

Marsch, E., von Steiger, R., & Bochsler, P. 1995, A&A, 301, 261

Mason, G. M., Mazur, J. E., Dwyer, J. R., Jokipii, J. R., Gold, R. E., & Krimigis, S. M. 2004, ApJ, in press

Mazzotta, P., Mazzitelli, G., Colafrancesco, S., & Vittorio, N. 1998, A&AS, 133, 403

McAteer, R. T. J., Gallagher, P. T., Bloomfield, D. S., Williams, D. R., Mathiuodakis, M., & Keenan, F. P. 2004, ApJ, 602, 436

McKenzie, J. F. 2000, Solar Physics, 196, 329

McKenzie, J. F., Sukhorukova, G. V., & Axford, W. I. 1997, A&A, 332, 367

Melrose, D. B. 1986, Instabilities in Space and Laboratory Plasmas, (Cambridge: Cambridge University Press)

Mewe, R., Kaastra, J. S., van den Ord, G. H. J., Vink, J., & Tawara, Y. 1997, A&A, 320, 147

Nakariakov, V. M., Ofman, L., DeLuca, E., Roberts, B., & Davila, J. M. 1999, Science, 285, 862

Ofman, L. 2002, ApJ, 568, L13

Peter, H. 1998, A&A, 335, 691

Peter, H., & Marsch, E. 1998, A&A, 333, 1069

Peter, H. 1996, A&A, 312, L37

Raassen, A. J. J., Mewe, R., Audard, M., Güdel, M., Behar, E., Kaastra, J. S., van der Meer, R. L. J., Foley, C. R., & Ness, J. -U. 2002, A&A, 389, 228

Raassen, A. J. J., Ness, J.-U., Mewe, R., van der Meer, R. L. J., Burwitz, V., & Kaastra, J. S. 2003a, A&A, 400, 671

Raasse, A. J. J., Mewe, R., Audard, M., & Güdel, M. 2003b, A&A, 411, 509

Reames, D. V. 2000, ApJ, 540, L111

Sanz-Forcada, J., Favata, F., & Micela, G. 2004, A&A, 416, 281

Sanz-Forcada, J., Maggio, A., & Micela, G. 2003, A&A, 408, 1087

Schwadron, N. A., Fisk, L. A., & Zurbuchen, T. H. 1999, ApJ, 521, 859

Vauclair, S., & Meyer, J.-P. 1985, Proceedings of 19th International Cosmic Ray Conference, 4, 233

Vernazza, J., Avrett, E. H., & Loeser, R. 1981, ApJS, 45, 635

Vernazza, J., & Reeves, E. M. 1978, ApJS, 37, 485

Verner, D. A., Ferland, G. J., Korista, K. T., & Yakovlev, D. G. 1996, ApJ, 465, 487

von Steiger, R., & Geiss, J. 1989, A&A, 225, 222

Watko, J. A., & Klimchuk, J. A. 2000, Sol. Phys. 193, 77

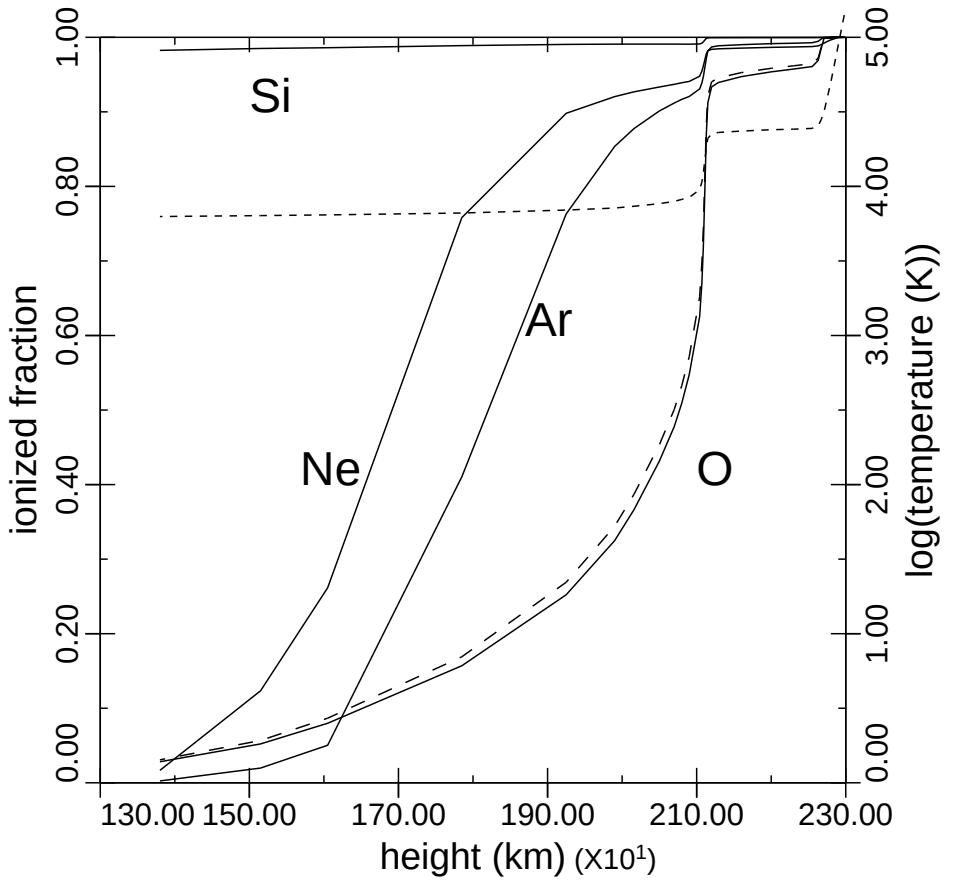

Fig. 1.— Plots of ionization fraction (solid lines) of Si, O, H, and Ne against height above the photosphere derived from model calculations. The long dashed line shows the H ionized fraction in the VALC model for comparison. The short dashed line, to be read on the right hand y-axis, gives the plasma temperature from VALC.

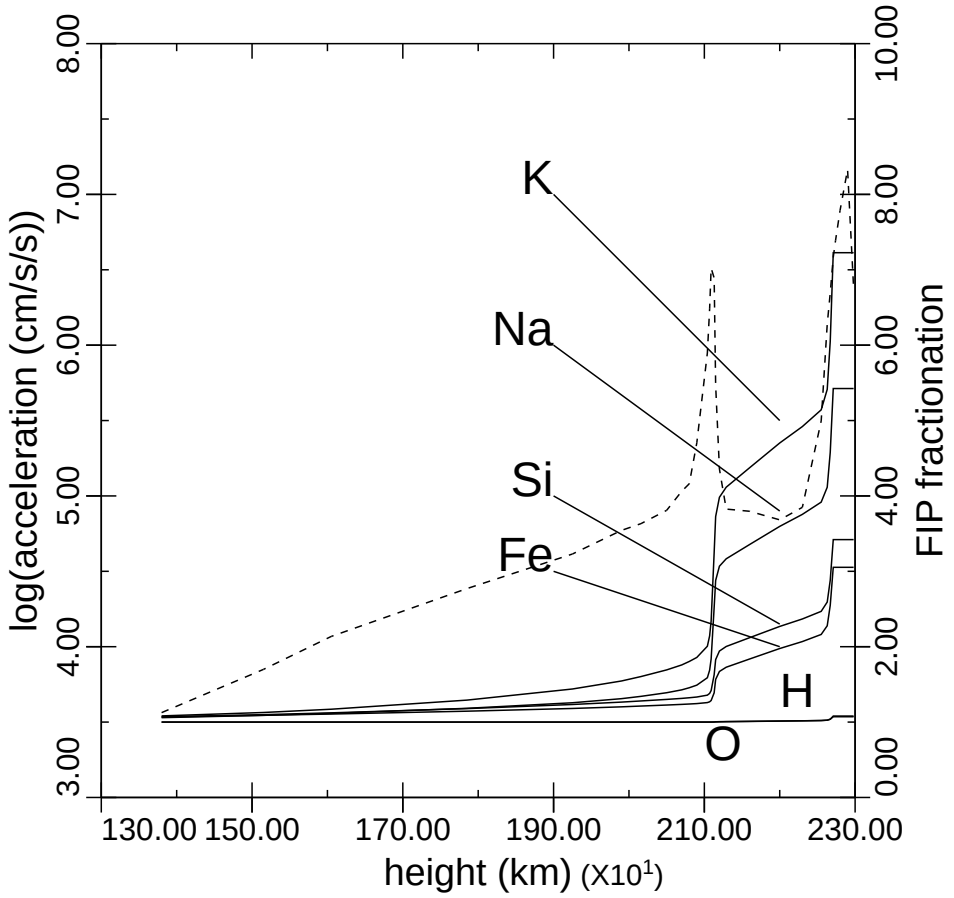

Fig. 2.— Plots of FIP fractionation against height (solid lines) for O, H, Fe, Si, Na, and K, to be read on the right hand y-axis. The dashed line gives the ponderomotive acceleration, read on the left hand y-axis. Low FIP enhancements where this acceleration is strong can clearly be seen. The wave energy density is 0.04 ergs cm^{-3}, corresponding to the quiet sun "reference" model.

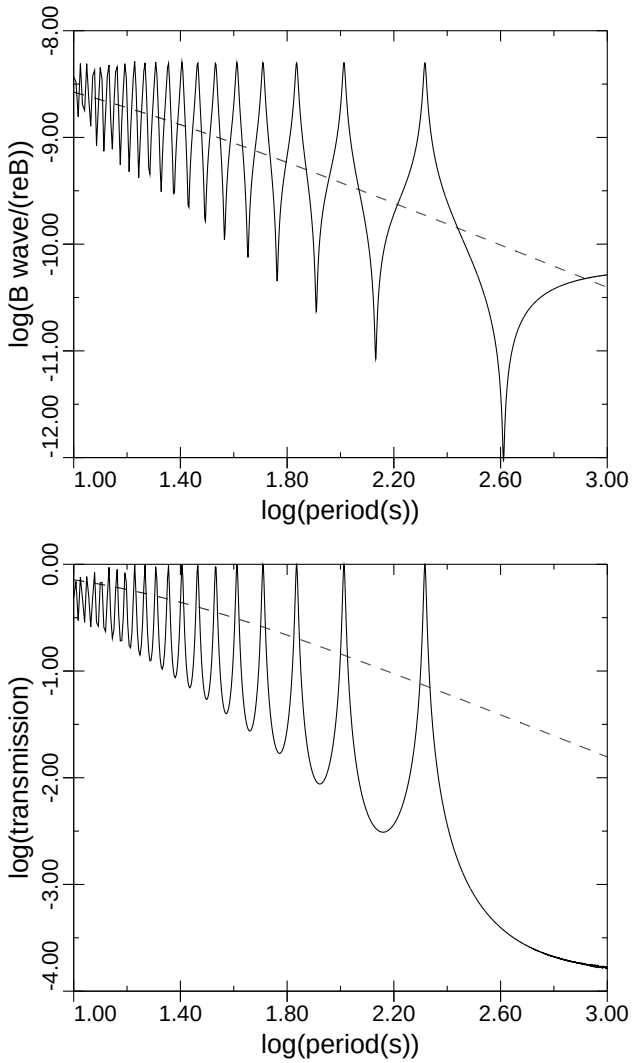

Fig. 3.— Plots of wave magnetic field at corona-chromosphere boundary (upper panel) and the Alfvén wave transmission into the corona from the chromosphere (lower panel) against wave period for a model solar chromosphere and corona (gravitational scale height 2×10^7 cm, coronal Alfvén speed 10^8 cm s^{-1}, and coronal loop length 10^{10} cm). Dashed curves show corresponding properties for a coronal hole (with loop length $\rightarrow \infty$). Strongest wave magnetic field and hence ponderomotive force is associated with transmission maxima. The absence of these maxima for the coronal hole leads to relatively weak ponderomotive force and hence essentially no FIP fractionation.

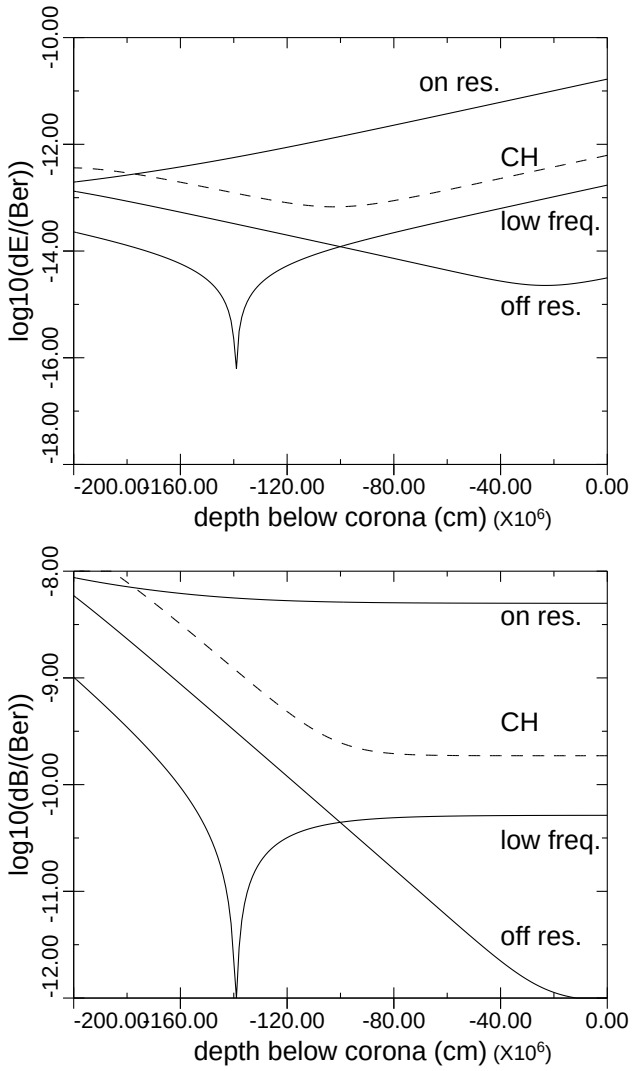

Fig. 4.— Plots of Alfvén wave electric field (upper panel) and magnetic field (lower panel), against distance below the chromosphere corona boundary for various wave periods; "on res." corresponds to the transmission maximum at 207 s period, "off res." to the transmission minimum at 408 s period, and "low freq." to a wave period of 1000 s. The ponderomotive force on ions is directed along the gradient of the wave electric field. The "on res." wave electric field increases with height throughout the chromosphere, giving an upwards ponderomotive force at all heights. Other wave periods give a combination of downwards ponderomotive force at low chromospheric heights and an upwards ponderomotive force higher up.

Table 1. Elastic Scattering Cross Sections with H

element	He	C	N	O	Ne	S	Ar
σ_{sn} (10^{-15} cm^2)	0.89	2.84	2.17	2.35	1.05	3.27	1.45

Table 2. FIP Fractionations for VALC

wave energy density (ergs cm^{-3}) element and FIP (eV)	0.01	0.02	0.028	0.04	0.057	0.08	0.113	obs.[a]
H (13.6)	1.02	1.03	1.05	**1.07**	1.10	1.15	1.21	
He (24.6)	1.00	1.00	1.01	**1.01**	1.01	1.02	1.02	
C (11.3)	1.04	1.07	1.10	**1.15**	1.22	1.33	1.50	
N (14.5)	1.04	1.08	1.11	**1.16**	1.24	1.35	1.54	
O (13.6)	1.02	1.04	1.06	**1.08**	1.11	1.17	1.24	
Ne (21.6)	1.02	1.05	1.07	**1.10**	1.14	1.20	1.31	
Na (5.1)	1.53	2.33	3.31	**5.42**	10.9	29.4	119	4-8
Mg (7.6)	1.36	1.85	2.39	**3.42**	5.70	11.7	32.5	4
Al (6.0)	1.33	1.76	2.23	**3.11**	4.98	9.69	24.8	4-8
Si (8.2)	1.36	1.85	2.39	**3.42**	5.69	11.7	32.4	4
S (10.4)	1.18	1.39	1.59	**1.93**	2.54	3.73	6.43	
Ar (15.8)	1.06	1.12	1.17	**1.25**	1.36	1.55	1.86	
K (4.3)	1.64	2.69	4.05	**7.22**	16.4	52.2	269.	11
Ca (6.1)	1.31	1.71	2.13	**2.91**	4.53	8.46	20.5	4-8
Fe (7.9)	1.32	1.75	2.20	**3.05**	4.85	9.32	23.5	4
Ni (7.6)	1.27	1.61	1.97	**2.60**	3.87	6.77	15.0	4
Kr (14.0)	1.04	1.08	1.11	**1.16**	1.23	1.34	1.52	
Rb (4.2)	1.71	2.95	4.62	**8.71**	21.3	75.8	455.	
W (8.0)	1.72	2.99	4.71	**8.95**	22.2	80.2	493.	

[a]Estimates in the final column are observed FIP fractionations quoted in Feldman & Laming (2000) and Feldman & Widing (2003).